Exchange interactions and high-energy spin states in Mn_{12}-acetate

G. Chaboussant,* A. Sieber, S. Ochsenbein, H.-U. Güdel, and M. Murrie
Departement für Chemie und Biochemie, Universität Bern, Freiestrasse 3, CH-3000 Bern 9, Switzerland

A. Honecker and N. Fukushima
Institut für Theoretische Physik, Technische Universität Braunschweig, Mendelssohnstr. 3, 38106 Braunschweig, Germany

B. Normand†
Département de Physique, Université de Fribourg, CH-1700 Fribourg, Switzerland
(Dated: April 8, 2004; revised June 27, 2004)

We perform inelastic neutron scattering measurements on the molecular nanomagnet Mn_{12}-acetate to measure the excitation spectrum up to 45 meV (500 K). We isolate magnetic excitations in two groups at 5–6.5 meV (60–75 K) and 8–10.5 meV (95–120 K), with higher levels appearing only at 27 meV (310 K) and 31 meV (360 K). From a detailed characterization of the transition peaks we show that all of the low-energy modes appear to be separate $S = 9$ excitations above the $S = 10$ ground state, with the peak at 27 meV (310 K) corresponding to the first $S = 11$ excitation. We consider a general model for the four exchange interaction parameters of the molecule. The static susceptibility is computed by high-temperature series expansion and the energy spectrum, matrix elements and ground-state spin configuration by exact diagonalization. The theoretical results are matched with experimental observation by inclusion of cluster anisotropy parameters, revealing strong constraints on possible parameter sets. We conclude that only a model with dominant exchange couplings $J_1 \sim J_2 \sim 5.5$ meV (65 K) and small couplings $J_3 \sim J_4 \sim 0.6$ meV (7 K) is consistent with the experimental data.

PACS numbers: 75.30.Et, 75.50.Xx, 78.70.Nx

I. INTRODUCTION

The topic of molecular magnets[1,2] has emerged in the last decade as one of the major interdisciplinary fields of research in the materials science community. Molecular magnets, also called "spin clusters", are crystalline materials composed of magnetic centers, mostly transition-metal ions, which have strong mutual interactions within each molecule. Each spin cluster in the lattice is magnetically well isolated from its neighbors due to the presence of surrounding ligands. This magnetic shielding allows the study of the individual behavior of nanometer-scale magnetic systems.

Chemists and physicists have combined efforts in an increasingly coordinated approach to develop and design new magnetic molecules which can show purely quantum properties at the macroscopic level. Such phenomena include very slow relaxation of the magnetization below the "blocking" temperature T_B.[3,4] and quantum tunneling of the magnetization vector through an energy barrier between "spin up" and "spin down" configurations.[5] The barrier Δ is governed, to leading order, by two parameters, the ground-state spin value S and the axial anisotropy $D \leq 0$ of the cluster, which yield $\Delta = -DS^2$. The magnetic properties of the molecules are determined primarily by the exchange interactions between individual ionic spins and by their magneto-crystalline anisotropy. Competition among the different exchange couplings can lead to a wealth of situations ranging from a nonmagnetic ground state ($S = 0$) to a variety of large-spin ground states ($S \geq 10$). A precise knowledge of the values of the exchange interactions, and their dependence on the geometry of the molecular cluster, is therefore critical to understand the ground state and, more generally, the possibilities for new synthetic procedures providing better materials with larger energy barriers.

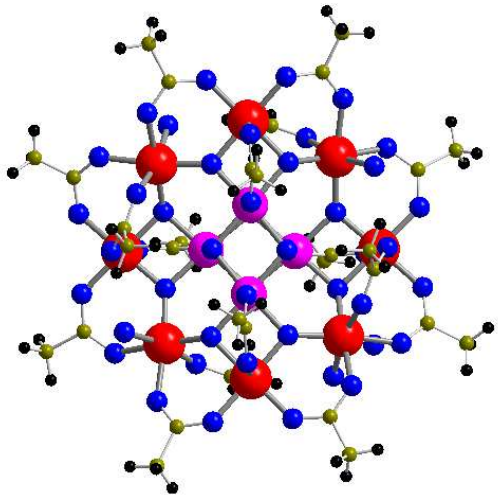

FIG. 1: (Color online) Structure of Mn_{12}-acetate viewed along the c axis. Large solid spheres represent Mn^{3+} ions (outer ring) and Mn^{4+} ions (inner core). All Mn atoms have a distorted octahedral coordination geometry.

Inelastic neutron scattering (INS) is a powerful experimental probe of magnetic excitations and ex-

change or anisotropy parameters in molecular magnetic clusters.[6–15] Here we investigate the high-energy magnetic states in the best-characterized molecular magnetic system to date, Mn_{12}-acetate, using INS in the energy range between 1 and 100 meV (10-1000 K) and with no external magnetic field. Comparison between our experimental results and numerical calculations enables us to estimate the exchange interaction parameters in the Mn_{12}-acetate cluster.

The manuscript is organized as follows. In Sec. II we review the structure and properties of Mn_{12}-acetate, experimental results, and attempts which have been made to understand the exchange interactions. In Sec. III we present the results of INS measurements performed on three different spectrometers, and use these to characterize the magnetic excitations. Section IV contains a theoretical analysis of the conventional exchange model for Mn_{12}-acetate by high-temperature series expansion techniques for the susceptibility and exact diagonalization to obtain the ground state and low-lying excited states, both refined by comparison with the existing data. A summary and conclusions are presented in Sec. V.

II. STRUCTURE AND PROPERTIES OF Mn_{12}-ACETATE

A. Structural Information

Mn_{12}-acetate[4,16–18] is a mixed-valence (Mn^{3+}/Mn^{4+}) compound where the magnetic ions are arranged in two groups: a central core composed of a tetrahedron of 4 Mn^{4+} ions ($S = 3/2$) and an external ring, or crown, of 8 Mn^{3+} ions ($S = 2$). Figure 1 shows the Mn_{12}-acetate cluster viewed along the c axis. The point group of the Mn_{12} molecule in the crystal structure is S_4. To simplify the analysis we make the additional assumption of fourfold rotation and reflection symmetry of the individual molecular clusters, and return later to a discussion of this approximation. Each cluster is only very weakly coupled to its neighbors, which are separated from each other by molecules of water and acetic acid, such that no long-range magnetic order has been found for temperatures as low as the mK range. Consequently, most of the experimental work performed at temperatures exceeding 1 K may be interpreted in terms of the properties of a single molecule. Neighboring Mn ions within a cluster are coupled in an intricate pattern by different types of μ-oxo bridge and by acetate bridges, as a result of which both antiferromagnetic (AFM) and ferromagnetic (FM) exchange interactions may be present in the system. A schematic representation of the exchange couplings is shown in Fig. 2. Within the approximation of fourfold cluster symmetry there are three inequivalent Mn sites with four different exchange couplings between neighboring Mn ions: J_1 (involving two μ-oxo bridges) and $J_2 = J_{2a} \approx J_{2b}$ (one μ-oxo bridge) between Mn^{3+} and Mn^{4+} ions, J_3 between Mn^{4+} ions inside the core tetrahedron (two μ-oxo bridges) and $J_4 = J_{4a} \approx J_{4b}$ between Mn^{3+} ions around the external ring (one μ-oxo bridge and two carboxylate groups). Inspection of the Mn-Mn distances and Mn-O-Mn angles presented in Table I suggests that the approximations $J_{2a} \approx J_{2b}$ and $J_{4a} \approx J_{4b}$ are eminently reasonable.

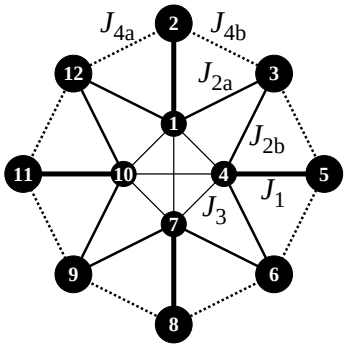

FIG. 2: Schematic representation of the magnetic exchange paths in Mn_{12}-acetate as first proposed by Sessoli *et al.*[16] J_1 couples Mn^{3+} and Mn^{4+} ions ($d = 2.771$ Å), $J_{2a,b}$ correponds to Mn^{3+}/Mn^{4+} ($d = 3.45$ Å), J_3 to Mn^{4+}/Mn^{4+} ($d = 2.817$ Å) and $J_{4a,b}$ to nearest-neighbor Mn^{3+} ions ($d = 3.33$ and 3.41 Å).

B. Ground State and Anisotropy

The magnetic ground state has a total spin $S = 10$, as first suggested by Sessoli *et al.*[16,17] and later confirmed by many experimental studies, including magnetization,[19] nuclear magnetic resonance (NMR),[20] electron paramagnetic resonance (EPR),[21,22] and INS[7] measurements. The $S = 10$ ground state may be rationalized by considering a ferrimagnetic arrangement of 8 parallel spins $S = 2$ on the crown Mn^{3+} ions oriented antiparallel to the 4 aligned $S = 3/2$ spins on the core Mn^{4+} ions.

While all of the Mn atoms have a distorted octahedral coordination geometry, the distortion is significantly stronger for the crown Mn^{3+} ions. The strongly nega-

TABLE I: Mn-Mn distances and μ-oxo bridge angles for the different exchange couplings in Mn_{12}-acetate. Mn pairs coupled by one μ-oxo bridge have greater separation ($d \geq 3.3$ Å) and a higher angle than those coupled by two μ-oxo bridges ($d \leq 3.3$ Å).

exchange path	Mn-Mn distance in Å	Mn-O-Mn angle
J_1	2.771	95.74°, 94.00°
J_{2a}	3.449	133.0°
J_{2b}	3.459	132.0°
J_3	2.817	95.2°, 95.0°
J_{4a}	3.331	122.52°
J_{4b}	3.410	129.15°

tive axial anisotropy parameter D of the cluster, which is due primarily to the Jahn-Teller distortion (axial octahedral elongation) around the Mn^{3+} ions, lifts the degeneracy of the $S = 10$ ground-state multiplet, with the $M_S = \pm 10$ states lying lowest. The $M_S = \pm 10$ and $M_S = 0$ states are separated by an energy barrier $\Delta = -DS_z^2$ of approximately 65 K (5.5 meV), which blocks the thermal relaxation in a typical magnetization relaxation experiment.[17,23–25] Surprisingly, the energy barrier Δ in Mn_{12}-acetate remains the highest known, despite intense efforts to synthesize new magnetic clusters.

Higher-order (rhombic and quartic) terms in the anisotropy are responsible for a mixing of wave functions between pairs of states of equal $|M_S|$ on either side of the barrier, opening a channel for tunneling through the barrier. This effect has been demonstrated and studied extensively in recent years by a variety of techniques, including low-temperature magnetometry,[19,26–28] NMR,[20] and specific heat.[23,29] An excellent determination of the quartic terms has been achieved using high-field EPR[21] and INS.[7] The recent discovery[30–32] of disorder in the acetic-acid and water molecules, which further lowers the site symmetry of some of the Mn_{12} clusters present in the lattice, has shed additional light on a long-standing controversy concerning the physical origin of the experimentally observed tunneling.[33–37]

With the primary aim of understanding the magnetic excitation spectrum, in this study we will treat the anisotropy contributions of single Mn ions using only phenomenological axial anisotropy parameters D_S^0 of the cluster spin S (D above denotes the ground-state anisotropy parameter, denoted D_{10}^0 in Sec. III F), and neglect all anisotropy terms of higher order than quadratic in single-ion or cluster spins. Because single-ion anisotropies are some two orders of magnitude smaller than the exchange couplings, and higher-order anisotropies smaller still, this treatment is expected to be acceptable. Nevertheless, approximations at the level of single-ion anisotropies do limit the accuracy with which experimental results may be fitted in a theoretical analysis.

C. Magnetic Excitations

While the low-temperature properties of Mn_{12}-acetate are well described by an isolated $S = 10$ ground state, to date very little is known about the higher excited states whose energies are determined directly by the exchange interactions (J_1, J_2, J_3, J_4). The first experimental information was provided by magnetization measurements at very high fields using an explosive compression technique which can access magnetic fields in excess of $H = 900$ T.[38,39] A series of peaks is observed between 300 T to 600 T in the field derivative dM/dH, suggesting important steps in the magnetization curve which may be interpreted in terms of crossovers from $S = 10$ to $S = 11$, $12, \ldots$, up to the maximum possible spin value of $S = 22$. Further information on the interaction parameters may be obtained from fits to the high-temperature part of the zero-field susceptibility. However, because the Curie-Weiss regime is not established even at 300 K,[16] and significant loss of solvent occurs at and above 308 K, it is difficult to draw a reliable conclusion from such fits without a theoretical treatment of the susceptibility which is valid also for lower temperatures. Such an analysis has not been performed previously, and will be presented in Sec. IV below.

Based on susceptibility and magnetization data alone, the unambiguous determination of exchange constants of similar magnitude in such ferrimagnetic systems is impossible. INS is a unique spectroscopic technique which can gather information over a wide energy range, and is thus capable of identifying a number of energy levels sufficient to evaluate the exchange interactions in complex systems such as Mn_{12}-acetate.

Hennion *et al.*[6], using an approximately 30% deuterated Mn_{12}-acetate sample, showed clearly for the first time that important higher-energy transitions were observable above the transitions within the ground-state multiplet. These authors reported a series of inelastic peaks between 4 meV and 10 meV (45–110 K) which were ascribed to transitions between the $S = 10$ ground state and $S = 9$ excited states. In this study we confirm the INS peaks observed in Ref. 6, providing more detailed information concerning these, and extend our survey to higher energies. Comparison between the experimental data and the spectra obtained from exact numerical diagonalization of a four-parameter model for the magnetic cluster allows us to assign the observed energy levels and to determine a consistent set of values for the exchange interactions in Mn_{12}-acetate.

D. Estimates of Exchange Interactions

The first theoretical attempts to determine the exchange interactions considered a simplified model[16,40–42] predicated on the assumption of a single AFM exchange interaction J_1 much larger than any of the other parameters in the system. In this situation the 4 Mn^{3+}-Mn^{4+} pairs coupled by J_1 are locked in their $S = 1/2$ ground state, and the size of the spin space is considerably reduced, namely to 4 spins $S = 1/2$ and 4 spins $S = 2$. Although this model provided a qualitative account of the available susceptibility data, it was far from providing a unique answer. Further, from qualitative considerations of exchange interactions, and particularly the proximity of the J_1 μ-oxo bridging angle to 90°, even this simplifying assumption lacks justification. In short, a fully general starting point is required, and the absence of detailed information concerning the location of the magnetic excitations precludes any unambiguous determination of the exchange couplings.

Several attempts have been made to evaluate the ex-

change interactions by applying numerical techniques, specifically exact diagonalization[43,44] and different variants of density functional theory (DFT) calculations,[45,46] to a model of the type discussed above. The results of these studies were then compared with a selectively chosen subset of the available data, taken from high-field magnetization,[38,39] a.c. susceptibility,[23,47] high-field EPR,[48] and INS[6] measurements, to argue in support of a particular parameter set. Raghu *et al.*[43] considered the parameters proposed in Ref. 16, and demonstrated that these do not in fact yield an $S = 10$ ground state. Variants on this set were tested which did satisfy this condition, but we will show below that the very large values of J_1 [215 K (18.5 meV)] and of J_2 and J_3 [85 K (7.3 meV)] are inconsistent with the measured susceptibility. Regnault *et al.*,[44] focusing on the $S = 10$ condition, obtained $J_1 = 119$ K (10.2 meV), $J_2 = 118$ K (10.2 meV), $J_3 = -8$ K (-0.69 meV), and $J_4 = 23$ K (1.98 meV), where the magnitudes of the parameters were determined by fitting the magnetization data. Park *et al.*[46] obtained a not dissimilar result in an *ab initio* DFT calculation, specifically $J_1 = 115$ K (9.91 meV), $J_2 = 84$ K (7.24 meV), $J_3 = -4$ K (0.34 meV), and $J_4 = 17$ K (1.47 meV). In both of these cases, J_1 and J_2 are rather close in value, in sharp contrast to the assumption underpinning the simplified, dimerized model. While J_1 is much smaller than previously suggested,[16] in combination with the larger J_2 value these sets also overestimate the high-temperature susceptibility quite considerably. The much weaker J_3 and J_4 interactions are then difficult to determine systematically, although both sets suggest that J_3 may be weakly FM. Finally, Boukhvalov *et al.*[45] obtained a smaller set of values, $J_1 = 47$ K (4.1 meV), $J_2 = 26$ K (2.2 meV), two different core-spin coupling terms $J_3 = 30$ K (2.6 meV) and $J_3' = 10$ K (0.86 meV), and $J_4 = 7$ K (0.60 meV). However, from our computations these last values appear to give neither a ground state with $S = 10$ nor a suitable reproduction of the magnetization.

It is thus clear that no consensus has yet emerged on the exchange coupling values in Mn_{12}-acetate. The objective of this study is to determine these exchange interactions based on the present INS results for the previously unexplored energy range up to 45 meV (500 K), in combination with information obtained from susceptibility and magnetization data. We will find that it is possible to determine an effectively unique set of interaction parameters capable of explaining consistently all of the available information, i.e. the $S = 10$ ground state, the high-temperature susceptibility, the approximate location of the observed magnetization steps, and the magnetic excitations measured by INS.

III. EXPERIMENT

A. Experimental Details

The INS experiments were performed on three different instruments located at three different sources: 1) the time-of-flight (TOF) spectrometer IN4 at the Institut Laue-Langevin (Grenoble, France) using wavelengths $\lambda = 1.1$ Å and 2.2 Å, 2) the TOF spectrometer FOCUS at the Paul Scherrer Institute (Villigen, Switzerland) using the wavelength $\lambda = 3.1$ Å, and 3) the MARI spectrometer at the pulsed neutron source ISIS (Didcot, UK) using neutrons with incident energies between 12 meV and 50 meV (in this section we quote energies only in meV). IN4 and MARI are best suited for high energy transfers and a wide Q-range, while FOCUS is a cold-neutron spectrometer designed for energy transfers below 5-10 meV. Data were collected at several temperatures between 1.5 K and 100 K, and corrected for the background and detector efficiency by means of a vanadium reference and empty-cell measurements for each incident energy.

On IN4 and FOCUS, we used a fresh, 3.8 g polycrystalline powder sample of fully deuterated Mn_{12}-acetate placed under helium in a flat, rectangular aluminum slab of 3 mm thickness. Full deuteration was achieved by systematic substitution of hydrogenated precursors with deuterated versions under argon. On MARI, the sample, wrapped in aluminum foil, was mounted in a hollow cylinder of diameter 42 mm and height 62 mm. The sample thickness was approximately 3 mm.

On IN4, the ^{3}He detector banks cover the angular range $2\theta = 13$-$120°$, giving access to momentum transfers $0.7 \leq Q \leq 4$ Å^{-1} at $\lambda = 2.2$ Å and $2 \leq Q \leq 9$ Å^{-1} at $\lambda = 1.1$ Å. The resolution obtained from a metallic vanadium reference, given as the full-width at half-maximum peak height of the elastic line, was $\Gamma = 0.9$ meV at 2.2 Å and $\Gamma = 3.8$ meV at 1.1 Å. On FOCUS, the detector banks cover the angular range $2\theta = 10$-$130°$, giving access to momentum transfers $0.7 \leq Q \leq 3.4$ Å^{-1} at $\lambda = 3.1$ Å. FOCUS is a time- and space-focusing TOF spectrometer which allows inelastic focusing. At an energy loss of approximately 5 meV, the resolution, obtained from a metallic vanadium reference, was $\Gamma = 0.4$ meV at 3.1 Å. On MARI, the detectors cover the angular range $2\theta = 12$-$135°$ and momentum transfers up to $Q \approx 8$-9 Å^{-1} for the highest energy transfer used (50 meV). The elastic resolution ranged from 0.15-0.2 meV at an incident energy $E_i = 12$ meV to 1 meV at $E_i = 50$ meV.

B. Magnetic Neutron Cross-Section

The differential magnetic neutron cross-section for a transition $|\Psi_m\rangle \rightarrow |\Psi_n\rangle$ is[49]

$$\begin{aligned}\frac{d^2\sigma}{d\Omega dE} &= \frac{N}{4}\left\{\frac{\gamma e^2}{m_e c^2}\right\}^2 \frac{k'}{k} e^{-2W(\boldsymbol{Q})} F^2(\boldsymbol{Q}) \\ &\times \sum_{\alpha,\beta}\left\{\delta_{\alpha\beta} - \frac{Q_\alpha Q_\beta}{\boldsymbol{Q}^2}\right\} \\ &\times \sum_{i,j} \exp^{i\vec{Q}\cdot(\vec{R}_i - \vec{R}_j)} \langle\Psi_m|\, \hat{S}_i^\alpha\, |\Psi_n\rangle \\ &\times \langle\Psi_n|\, \hat{S}_j^\beta\, |\Psi_m\rangle\, \delta\left(\hbar\omega + E_n - E_m\right). \end{aligned} \quad (1)$$

In this equation N is the number of Mn_{12} molecules in the sample, k and k' are the wavenumbers of the incoming and scattered neutrons, $\boldsymbol{Q}$ is the scattering vector, $\exp(-2W(\boldsymbol{Q}))$ is the Debye-Waller factor, $\hbar\omega$ is the neutron energy, $|\Psi_m\rangle$ are the cluster wave functions with energies E_m, $F(\boldsymbol{Q})$ is the magnetic form factor, $\vec{R}_i$ is the space vector of the ith Mn ion in the cluster, α and β represent the spatial coordinates x, y, and z, e and m_e are respectively the charge and mass of the electron, c is the speed of light, and $\gamma = -1.91$ is the gyromagnetic constant of the neutron. INS selection rules impose that the matrix elements in Eq. (1) are nonzero only when $\Delta S = S - S' = 0, \pm 1$ and $\Delta M_S = M_S - M_S' = 0, \pm 1$ where the initial and final states are defined respectively by (S, M_S) and (S', M_S').

C. Energy-dependence

Figure 3 shows inelastic spectra obtained on MARI at $T = 8$ K at three different incident energies ($E_i = 50, 17,$ and 12 meV). Several transitions are observed between 1.2 meV and 32 meV. At $E_i = 50$ meV [Fig. 3(a)], four sets of transitions are visible above a broad background produced by incoherent scattering. These sets are labeled (I) to (IV), and their peak energies are 5.3, 8.5, 27, and 31 meV, respectively. The positions of (I) and (II) are consistent with the observations made by Hennion *et al.*[6]

Figure 3(b), corresponding to $E_i = 17$ meV, shows that peaks I and II are composed of several components. These are labeled (Ia), (Ib), (IIa), (IIb), and (IIc), and from the center lines of Gaussian fitting curves appear respectively at energies of 5.15, 6.04, 7.90, 8.64, and 9.73 meV. While a double-peak structure is clearly established for transitions (Ia) and (Ib), it is less obvious for the higher-energy transitions. The peaks were fitted using Gaussian lineshapes by assuming a constant line width $\Gamma \approx 0.75$ meV for all transitions and a linearly decreasing slope to account for the background. The width is determined from transitions (Ia) and (Ib) and its value is maintained for the other transitions. This is again in qualitative agreement with Fig. 8 of Ref. 6.

Figure 3(c) confirms clearly that there is an energy splitting between transitions (Ia) and (Ib) but transitions (IIa) and (IIb) remain (barely) unresolved. At this value of E_i the width of these transitions is between 0.45 and 0.55 meV. Based on its Q- and T-dependence (not shown), the broad peak around 2.65 meV may be attributed to phonon excitations. In addition, with this resolution it is now possible to observe the transition peak within the ground state, labeled (GS1), at $\hbar\omega \approx 1.25$ meV, in complete agreement with the results of Mirebeau *et al.*[7] This peak is significantly sharper ($\Gamma \approx 0.35$ meV) than the higher-energy transitions, suggesting an

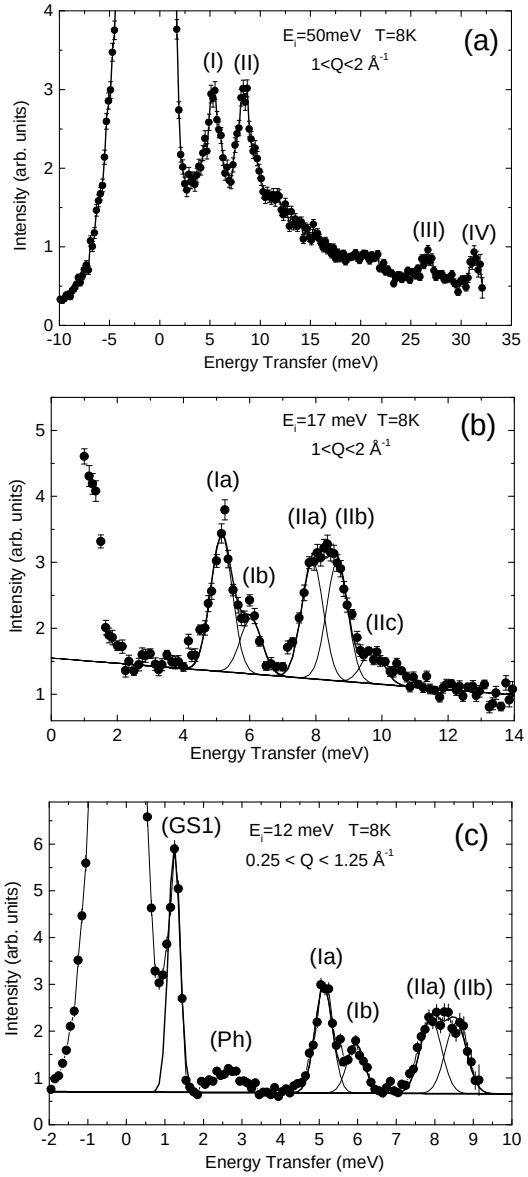

FIG. 3: INS spectra obtained at $T = 8$ K on MARI at (a) $E_i = 50$ meV, (b) $E_i = 17$ meV, and (c) $E_i = 12$ meV. The Q-range is restricted to $1 \leq Q \leq 2$ Å^{-1} in panels (a) and (b) and to $0.25 \leq Q \leq 1.25$ Å^{-1} for panel (c). Transitions are labeled as discussed in the text. In panel (c), (GS1) is a transition within the $S = 10$ ground-state multiplet and (Ph) denotes a low-energy phonon mode.

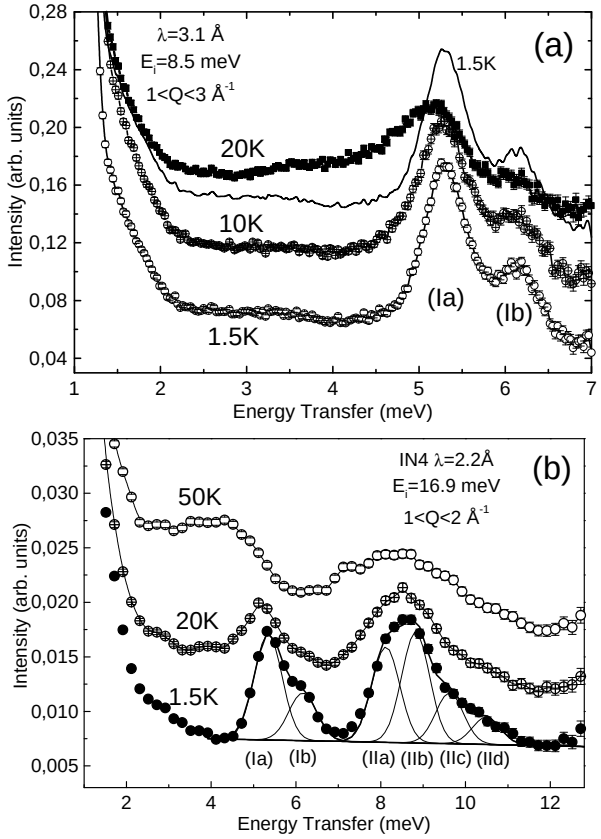

FIG. 4: (a) Inelastic spectra at $T = 1.5$ K, 10 K, and 20 K obtained on FOCUS at an incident wavelength $\lambda = 3.1$ Å. At 1.5 K, transitions (Ia) and (Ib) are observed at $\hbar\omega = 5.3$ meV and $\hbar\omega = 6.2$ meV, respectively. The data taken at 1.5 K are reproduced as a solid line and shifted upwards to facilitate comparison with the 20 K data.(b) Inelastic spectra at $T = 1.5$ K, 20 K, and 50 K obtained on IN4 at $\lambda = 2.2$ Å.

intrinsic line-broadening of transitions (Ia) to (IIb).

D. *T*-dependence

Figure 4(a) shows the inelastic spectra obtained on FOCUS at temperatures of 1.5 K, 10 K, and 20 K, after integrating over a group of detectors such that the Q-range is $1 \leq Q \leq 3$ Å^{-1}. A vertical offset is applied between the curves for clarity. The results provide a significant improvement in the understanding of transitions (Ia) and (Ib): these have energies of $\hbar\omega_{Ia} \approx 5.3$ meV and $\hbar\omega_{Ib} \approx 6.2$ meV at 1.5 K, consistent with the MARI data (taken at 8 K). As the temperature is increased there is a shift of both peaks towards lower energies, and some broad scattering develops below 5 meV. This is shown clearly by comparison of the data taken at 20 K and 1.5 K (solid line), for which the same vertical offset is applied. The shift to lower energies arises from progressive population of the higher M_S sublevels in the $S = 10$ ground-state multiplet, which results in a large number of

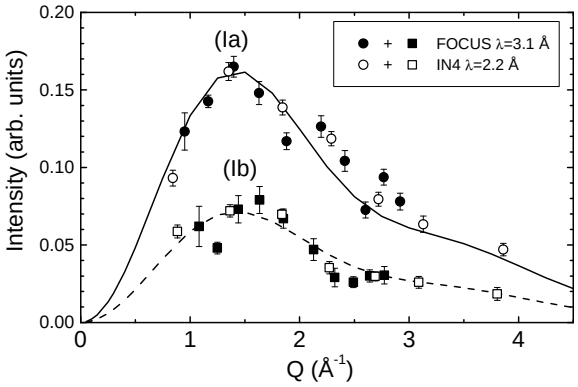

FIG. 5: Q-dependence at 1.5 K of peaks (Ia) and (Ib) obtained from the inelastic spectra shown in Fig. 4(a). Data from both FOCUS and IN4 are shown after normalization of the maximum intensity at $Q \approx 1.45$ Å^{-1}.

new magnetic transitions visible by INS and permits an estimate of the anisotropy splitting in the excited states (see Sec. III F).

Figure 4(b) presents inelastic spectra obtained on IN4 over a range of temperatures between 1.5 K and 50 K, where the Q-range is limited to $1 \leq Q \leq 2$ Å^{-1}. At 1.5 K one finds the transitions discussed above, which weaken progressively as the temperature increases, and finally merge into a single, broad feature in which both magnetic and phonon scattering are present. A general shift of intensity to lower energies is observed with increasing temperature for both peaks groups I and II. For the low-temperature data, by keeping the line width fixed to the value obtained by fitting transitions (Ia) and (Ib), $\Gamma = 0.77$ meV, the best fit to the large band at higher energies is obtained by considering four peaks, (IIa) to (IId), with energies of 8.1, 8.8, 9.6, and 10.5 meV. The first three peaks are globally consistent with the data from MARI [Fig. 3(b)]. However, the final peak, (IId), is very weak and does not seem to be present in the MARI data, so its existence must be said to be questionable.

E. *Q*-dependence

We consider next the Q-dependence of transitions (Ia) and (Ib). The integrated intensity is shown in Fig. 5 for the two transitions, with the FOCUS data represented by solid circles and squares, and the equivalent IN4 data by open symbols. Each integrated intensity point was obtained by fitting the peaks using a Gaussian function whose center, width, and intensity were all allowed to float.

For both peaks, the intensity passes through a maximum at $Q \approx 1.45$ Å^{-1}, and decreases progressively at higher Q values. This Q-dependence is typical of magnetic scattering, where the intensity is expected to follow the magnetic form factor $|F(Q)|^2$, a rapidly decreasing function above $Q \approx$ 2-3 Å^{-1}, modulated by a structure

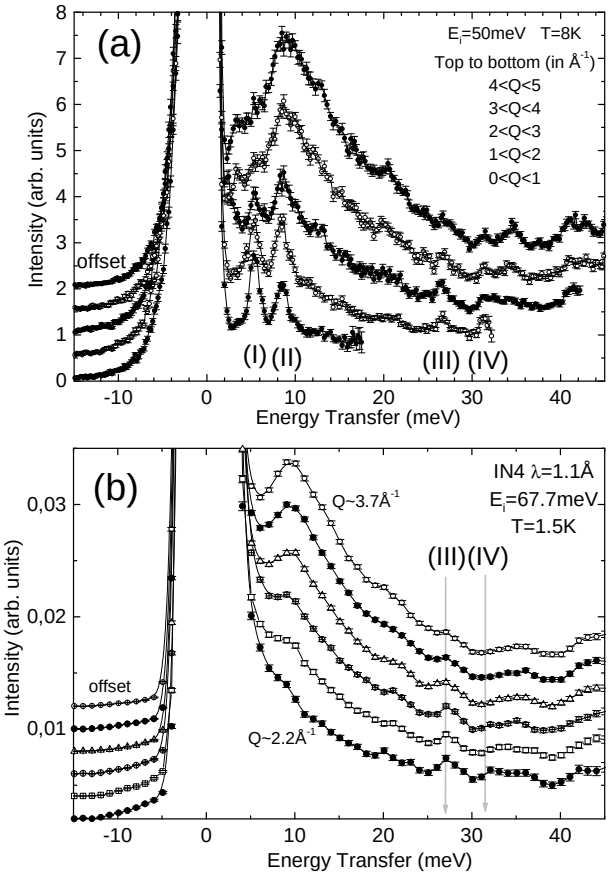

FIG. 6: (a) INS spectra obtained on MARI at $E_i = 12$ meV and $T = 8$ K for different values of Q. (b) INS spectra from IN4 at $\lambda = 2.2$ Å and $T = 1.5$ K for different values of Q.

form factor $I(Q)$ which depends on the exchange couplings and the exchange connectivity within the cluster.[50] In the simplest exchange-coupled system, a dimer, the structure form factor is given by[50]

$$I(Q) \sim \left(1 - \frac{\sin(QR)}{QR}\right), \qquad (2)$$

where R is the inter-atomic distance in the dimer. Using the dimer expression as an approximate indication, the maximum observed at $Q \approx 1.45$ Å^{-1} corresponds to $R \approx 2.8$ Å, a value close to the shortest Mn-Mn separation in Mn_{12}-acetate, $d = 2.77$ Å. By comparison, the Q-dependence of the ground-state transition at 1.25 meV is peaked at $Q \approx 0.95$ Å^{-1},[6] consistent with its different physical origin.

Figures 6(a) and (b) show the behavior of the INS spectra obtained respectively on MARI and IN4 over the full Q-range of each instrument. In both cases, the low-energy transitions (I) and (II) discussed above are lost rapidly in the incoherent phonon background as Q increases. The Q-dependence of peaks (III) and (IV) is more difficult to determine due to their weak intensity, but it is consistent with transitions of magnetic origin in that the intensity decreases with increasing Q. It is clear from both panels of Fig. 6 that the 27 meV peak is more pronounced at small Q values. A general increase of scattering is observed as Q is increased for all energies between 10 and 45 meV, which unfortunately impedes a complete analysis.

F. Assignment of Magnetic Peaks

Several magnetic peaks have been observed in four groups with energies $\hbar\omega_l$ as shown in Table II. For transitions (Ia) and (Ib), a detailed analysis may be performed of their dependence on Q and on temperature; for the higher transitions, only a more qualitative treatment is possible with the present data.

To determine the nature of these transitions, we begin by noting that due to the negative axial zero-field splitting only the $M_S = 10$ component of the $S = 10$ ground state is populated (over 99.5%) at 1.5 K, and therefore that only INS transitions from the state $(10, \pm 10)$ can be observed. From the selection rules in Sec. III B, it follows that only states with $S = 9, 10$, and 11 can be excited by INS, a clear example of which is the observation[7] of the transition from $E(10, \pm 10)$ to $E(10, \pm 9)$ within the $S = 10$ ground-state multiplet at $\hbar\omega \approx 1.25$ meV [peak (GS1) in Fig. 3(c)]. This result leads to the accurate determination of the axial anisotropy parameter for the $S = 10$ ground state, $D^0_{10} = -0.0566$ meV.

The assignment of spin states for the excited energy levels depends both on experimental observation and on certain assumptions concerning the axial anisotropy parameters for these states. We present first our treatment of anisotropy parameters, followed by the experimental results and a discussion of the consistency of this approach, which leads to the spin assignments shown in Table II. As noted in Sec. II B and discussed in greater detail in Sec. IV, given the nature of the data and the energy scales involved we restrict our considerations to the level of anisotropy parameters of the total spin. The canonical energy-level splitting for a given S state may be expressed as

$$E(S, M_S) = D_S \left(M_S^2 - \tfrac{1}{3}S(S+1)\right), \qquad (3)$$

TABLE II: Summary of energies and spin states of the observed magnetic transitions.

l	$\hbar\omega_l$	Properties
Ia	(5.3 ± 0.1) meV	$S = 9, M_S = \pm 9$
Ib	(6.2 ± 0.1) meV	$S = 9, M_S = \pm 9$
IIa	(8.0 ± 0.1) meV	$S = 9, M_S = \pm 9$
IIb	(8.7 ± 0.1) meV	$S = 9, M_S = \pm 9$
IIc	(9.7 ± 0.1) meV	$S = 9, M_S = \pm 9$
IId	(10.5 ± 0.1) meV	not confirmed
III	(27 ± 1) meV	$S = 9$, 10, or 11
IV	(31 ± 1) meV	may be magnetic

where D_S is the axial anisotropy parameter of the cluster in spin state S. We will not attempt to compute the anisotropy parameters D_S from vector coupling of the individual single-ion anisotropy terms, but for a qualitative interpretation of our observations will use related considerations to deduce their values relative to the measured ground-state axial anisotropy parameter D^0_{10}. In the absence of experimental information on this point, we begin by assuming that D_S is the same for all excited states of the same spin S, and return below to a more detailed consideration of this approximation.

A qualitative picture of the relative values of D^0_S for the lowest-energy states of each spin S in the Mn_{12}-acetate cluster may be obtained from a crude model based on two observations. From our approximation to the crystallographic symmetry all single-ion anisotropy terms are identical for both types of ion, and from the Jahn-Teller distortions these are very much greater for the 8 Mn^{3+} sites than for the 4 Mn^{4+} sites. A vector-coupling calculation of the spin state anisotropy performed only for the Mn^{3+} crown sites gives a systematic decrease of $|D^0_S|$ with decreasing S, and no change in the sign. In this elementary approach the anisotropy parameter deduced for $S = 9$ states, assumed to be composed of 3 Mn^{3+}-Mn^{3+} pairs with $S = 4$, one such pair with $S = 3$, and an antiparallel $S = 6$ core, is approximately 8% smaller than that for the $S = 10$ ground state. From a comparison with the coefficient $D^0_{10} = -0.0566$ meV extracted from INS data in Ref. 7, this result is fully consistent with the value $D^0_9 \approx -0.049$ meV estimated by fitting the magnetization to a similar dimerized model.[51]

For the uniaxial anisotropy parameter of the lowest excited $S = 11$ states, the simplest argument is to view these as a fully aligned $S = 16$ crown of Mn^{3+} ions, with changes of spin state from the $S = 10$ ground state occuring on the core Mn^{4+} ions, which have a very small single-ion anisotropy, whence $D^0_{11} \approx D^0_{10}$. The vector-coupling scheme above gives a value for D^0_{11} somewhat larger than D^0_{10}, but there is no qualitatively significant change in size or sign. The most important difference between $S = 9$ and $S = 11$ excited states for our purposes is that the latter should show three excitation branches corresponding to the (S, M_S) final states $(11, \pm 11)$, $(11, \pm 10)$, and $(11, \pm 9)$. These should be similar in intensity (differing by less than one order of magnitude) and should have a total energy span $\Delta E_{11} = 40 D^0_{11}$ [see Eq. (3)].

We now demonstrate that the temperature-dependence of magnetic peaks (I) is consistent with transitions from the ground state $(10, \pm 10)$ to excited states with $S = 9$ and $M_S = \pm 9$. The Q-dependence of the magnetic transitions at $\hbar\omega_{Ia} = 5.3$ meV and $\hbar\omega_{Ib} = 6.2$ meV is shown in Fig. 5. The decrease of intensity at low Q values is typical of transitions with $\Delta S = \pm 1$, which have zero intensity at $Q = 0$.[50] In contrast, transitions with $\Delta S = 0$ are strong at $Q = 0$. Further, as the temperature increases (Fig. 4) there is a growing scattering intensity below $\hbar\omega_{Ia}$. This suggests that additional magnetic transitions are emerging because the increasing temperature causes thermal population of more M_S sublevels of the $S = 10$ ground-state multiplet. From the value and sign expected for the parameter D^0_9, such a situation is possible only if the excited states corresponding to transitions (Ia) and (Ib) are two separate $S = 9$ states.

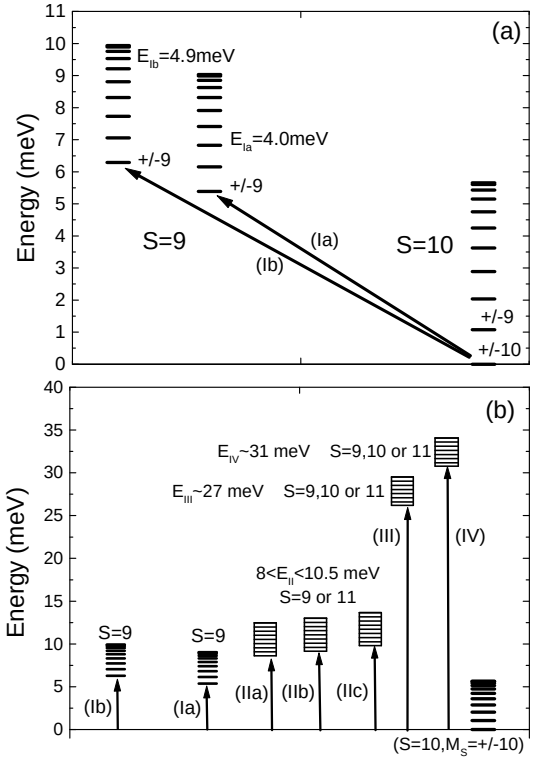

FIG. 7: (a) Detail of the low-energy levels inferred from our INS data (see text). After subtraction of the anisotropy shift, the lowest $S = 9$ states appear at 4.0 meV and 4.9 meV above the $S = 10$ ground state. (b) Energy levels observed by INS over the full range investigated. The spin values and anisotropy parameters of the higher levels are not known precisely.

By applying Eq. (3), the energies of transitions from the ground state $(10, \pm 10)$ to $S = 9$ spin states with $M_S = \pm 9$ can be written in the form

$$\begin{aligned} \hbar\omega_\alpha &= E(9, \pm 9) - E(10, \pm 10) \\ &= E_\alpha + \tfrac{190}{3}|D^0_{10}| - 51|D^0_9|, \end{aligned} \qquad (4)$$

where E_α is the energy of the $S = 9$ state in the absence of anisotropy. The multiplet structures are illustrated in Fig. 7(a), which shows also that the energy spread within the ground-state multiplet $(100 D^0_{10})$ is larger than that within the $S = 9$ manifolds $(81 D^0_9)$. As temperature increases, the state $(10, \pm 9)$ and other, higher states within the $S = 10$ multiplet are populated progressively and give rise to more INS transitions, which will necessarily occur at lower energies.

The measured changes in intensity can be fitted with semi-quantitative accuracy using the value $D^0_9 = -0.045$ meV, and in fact our data suggest that the result of Ref. 51 should be regarded as an upper bound. With

these cluster anisotropy parameters, the energetic shift induced in the transitions between the lowest $S = 10$ and $S = 9$ states is then

$$\hbar\omega_\alpha \approx E_\alpha + 1.29 \text{ meV}. \quad (5)$$

By contrast, if the excited states were of spin $S = 11$, for a reasonable value of D^0_{11} one would expect the opposite process (stronger scattering at higher energies), which is clearly precluded by the present data. Further, an explanation based on one or more $S = 11$ state(s) would require either a third excitation peak or that D^0_{11} be very much smaller than D^0_{10} so that all of the three peaks could be contained within the resolution width of the measurement; both of these possibilities may be excluded.

The situation is less clear regarding transitions (IIa-d) between 8 and 10.5 meV: it is evident from their evolution with temperature and with Q that these are magnetic excitations. The intensity peaks undergo a small shift towards lower energies as the temperature is increased [Fig. 4(b)], while their wavevector-dependence (not shown) appears to have a weak maximum at intermediate Q. In principle these transitions could correspond to final states with $S = 9, 10$ or 11. However, the combined T- and Q-dependence suggests that an $S = 10$ state is unlikely. In distinguishing between $S = 9$ and 11 states one may invoke both the weak T-dependence in combination with expected values for D^0_{11}, and the fact that the magnetization data of Refs. 38,39 do not appear to show a transition to an $S = 11$ state below a field of 200 T, implying that the first candidate $S = 11$ peak in the INS data would be (III). Thus from the qualitative similarity in behavior of peaks (II) with peaks (I), we assign peaks (II) to transitions with $S = 9$ final states. In Sec. IV we will show that a numerical analysis of the Mn_{12}-acetate exchange model confirms this assignment, and can be used to exclude the possibility of a set of $S = 11$ transitions with D^0_{11} significantly different from D^0_{10}.

We comment briefly on the assumption that the cluster anisotropy parameters D_S have the same value for all states of the same total spin S. We have used a simple model based on the classical spin arrangement of the $S = 10$ ground state and the strong difference in single-ion anisotropies between Mn^{3+} and Mn^{4+} ions to offer a consistent interpretation of all of the measured INS data. A small extension of this scenario is to consider the cluster as 4 Mn^{3+}-Mn^{3+}-Mn^{4+} trimer units, constructing the ground state from 4 $S = 5/2$ trimers and excited states as perturbations about this. Under the same assumption concerning single-ion anisotropies, one obtains a range of values of D_9 for different $S = 9$ states from 5% to 100% of D^0_{10}; for excited $S = 10$ and $S = 11$ states, the values of D_{10} and D_{11} range from 40% to 80% of D^0_{10}. While this analysis is far from systematic, it illustrates three important qualitative features. First, it is difficult to find states with $D > D^0_{10}$, a result which is not surprising given the fully aligned crown spins in this state, and helps to verify the assumptions underlying the interpretation. Second, the sign of D is always the same, suggesting that the temperature-dependence of the observed peaks can be used as a reliable indicator of the magnitude of D_S. Finally, this magnitude may in fact depend rather strongly on S; however, the constant sign is sufficient to ensure that the conclusions we have drawn from our INS data are robust against such quantitative changes.

In conclusion, the Q-dependence of transitions (Ia) and (Ib) corresponds to transitions from the $S = 10$ ground state to $S = 9$ final states, and not to $S = 11$ or other $S = 10$ states. While a similarly quantitative analysis is not possible for the transitions (IIa-d), we have obtained sufficient evidence to conclude that these are also of $S = 9$ character. For transitions (III) and (IV) a detailed investigation is excluded, and, on the basis of the general intensity decrease with increasing Q, we state only that these are of magnetic origin. A summary of the magnetic excitations identified by INS, their energies, and their S values is presented in Table II, and a graphical representation is provided in Fig. 7(b).

IV. MODEL ANALYSIS

The microscopic Hamiltonian for exchange interactions between individual Mn ions in the Mn_{12}-acetate cluster (Fig. 2) may be expressed as

$$\begin{aligned} H \;=\; \sum_{j=1}^{4} \{ & J_1\, \vec{S}_{3j-2} \cdot \vec{S}_{3j-1} + J_3\, \vec{S}_{3j-2} \cdot \vec{S}_{3j+1} \\ & + (J_2\, \vec{S}_{3j-2} + J_4\, \vec{S}_{3j-1}) \cdot (\vec{S}_{3j-3} + \vec{S}_{3j}) \} \\ & + J_3 (\vec{S}_1 \cdot \vec{S}_7 + \vec{S}_4 \cdot \vec{S}_{10}), \end{aligned} \quad (6)$$

with periodic boundary conditions $i \equiv i+12$. Sites $i = 1$, 4, 7, and 10 represent the core $S = 3/2$ spins on the Mn^{4+} ions, with mutual interactions J_3, and the other sites correspond to the $S = 2$ crown spins (Mn^{3+}), which have exchange interactions J_1 and J_2 with different core spins and J_4 with each other around the outer ring (Fig. 2). As stated in Sec. II A, we neglect other possible exchange paths, and assume despite the small structural distortions that the system is close to full fourfold rotation and reflection symmetry, and thus that $J_{2a} = J_{2b} = J_2$ and $J_{4a} = J_{4b} = J_4$. We will return later to a quantitative statement on this latter point. For the numerical analysis to follow we will not consider single-ion anisotropy terms around individual ions, which are instead included through the term in Eq. (3) for the spin states of the cluster. We will also discard any of the possible higher-order anisotropy terms, such as those of the form $B^0_4\, S^4_z$ and $\frac{1}{2} B^4_4 \left(S^4_+ + S^4_- \right)$. These approximations may be justified on the grounds of the small energy scale of the terms involved in comparison with the scale of the magnetic excitation spectrum (Sec. III).

The aim of this section is to determine a set of exchange constants $\{J_i\}$ which is capable of explaining the

magnetic excitation spectrum measured in Sec. III. Spectra of low-lying magnetic excitations have been tabulated by Raghu *et al.*[43] by considering a variety of parameter sets. It is evident from this analysis that none of the sets considered yields sufficiently many excitations with appropriate total spin below an energy of approximately 300 K (30 meV) to explain the INS results. Similarly, the excitation spectra computed for the parameter set of Ref. 44 also fails to provide a sufficient number of low-lying excitations to account for the new INS data (although we note here that these contain rather more levels in the relevant energy range than previous authors were aware of). While the parameter set of Ref. 46 is not inconsistent with the excitation spectrum, we will find in Sec. IV B that it cannot account for the magnetic susceptibility data. Hence the parameter sets discussed in Sec. II D are all incompatible with the experimental data. We therefore begin with an unbiased determination of an appropriate set of exchange constants $\{J_i\}$ by considering the ground state of the system using the full available parameter space. Candidate parameter sets are tested by computing the magnetic susceptibility, which we compare with our own measurements in Sec. IV B. In Sec. IV C we comment briely on the high-field magnetization data. We return to the issue of magnetic excitations in Secs. IV D and IV E, where we present a theoretical analysis of the energy spectrum of the cluster.

A. Numerical Methods

The numerical results are obtained by two methods. We have performed a systematic high-temperature series expansion to compute the magnetic susceptibility

$$T\chi(T) = C_0 + C_1\beta + C_2\beta^2 + C_3\beta^3 + C_4\beta^4 + \ldots, \quad (7)$$

where $\beta = 1/k_{\rm B}T$ with $k_{\rm B}$ the Boltzmann constant. For illustration, the first four coefficients C_n for the cluster geometry and ionic spins of Mn_{12}-acetate are given by

$$\begin{aligned}
C_0 &= 21, \\
C_1 &= -20J_1 - 40J_2 - \tfrac{75}{4}J_3 - 64J_4, \\
C_2 &= -5J_1^2 + 80J_1J_2 + 55J_2^2 + 75J_1J_3 + 150J_2J_3 \\
&\quad + \tfrac{675}{16}J_3^2 + 80J_1J_4 + 160J_2J_4 + 112J_4^2, \\
C_3 &= \tfrac{211}{6}J_1^3 + 20J_1^2J_2 - 80J_1J_2^2 + \tfrac{17}{6}J_2^3 - \tfrac{225}{4}J_1^2J_3 \\
&\quad -300J_1J_2J_3 - 325J_2^2J_3 - \tfrac{675}{4}J_1J_3^2 - \tfrac{675}{2}J_2J_3^2 \\
&\quad - \tfrac{405}{64}J_3^3 + 20J_1^2J_4 - 380J_1J_2J_4 - 280J_2^2J_4 \\
&\quad -300J_1J_3J_4 - 600J_2J_3J_4 - 140J_1J_4^2 \\
&\quad -280J_2J_4^2 - \tfrac{256}{15}J_4^3. \qquad (8)
\end{aligned}$$

One observes that C_0 is a constant, C_1 a weighted sum of the cluster interactions, C_2 a sum of certain combinations of squares, and so on. We have continued the series to 8th order, where the expressions are best handled by symbolic computation methods,[52] and have included the full Mn_{12} cluster rather than employing a conventional linked-cluster expansion.

The second method we employ is the calculation of low-lying excitations for a given set of input interaction parameters $\{J_i\}$ by exact diagonalization (ED) of the cluster Hamiltonian (6) using the Lanczos procedure. We have used the conservation of S_z, the z-component of the total spin, as well as the spatial symmetries of the cluster. Conservation of S_z is particularly important in reducing the dimension of the Hamiltonian matrix and is one of the reasons for which we do not include single-ion anisotropy terms in Eq. (6). Spatial symmetries of the states are denoted by a "momentum" k such that a state acquires a factor $\exp(ik)$ under a 90° rotation of the model for the Mn_{12} cluster shown in Fig. 2. We have used in addition the reflection symmetries of the cluster for $k = 0$ and $k = \pi$. For the description of the INS results, and to test whether the spin of the ground state is $S = 10$, one must consider at least the sectors with $S_z \geq 9$. The largest matrix dimension is then 324 908, which occurs for $S_z = 9$, $k = \pi/2$. This dimension is sufficiently small that rapid diagonalization by the Lanczos procedure is possible on a modern personal computer. Indeed, fast diagonalization is a necessary condition for an analysis requiring the consideration of many sets of parameters $\{J_i\}$. Finally, using our optimal parameter set we have performed further computations with $S_z = 0$ to ensure that the spin of the ground state is indeed $S = 10$. For $S_z = 0$ the largest dimension to be considered is 1 073 763 when using spin inversion symmetry.

The condition of a ground state with spin $S = 10$ already sets a strong constraint on the ratios of the exchange interactions, and, for example, may be used to exclude the parameter sets proposed in Refs. 16 and 45. We have computed low-energy spectra for approximately 1500 independent parameter sets which satisfy the $S = 10$ ground-state condition. Many of these sets were considered in Ref. 44, but we have performed independent computations for all parameter sets and added further points in regions indicated by the susceptibility calculation as potentially relevant. We note that the $S = 10$ condition is invariant under rescaling of the interaction parameters, whence one obtains a line in the four-dimensional parameter space from each independent diagonalization.

B. Magnetic Susceptibility

The behavior of the static susceptibility of a magnetic material at high temperatures may be used in a systematic manner to extract information concerning the exchange interactions within the system (see for example Ref. 53). The simplest example of this process is that the first correction to paramagnetic behavior in a FM or AFM system gives the Curie-Weiss temperature, which is directly proportional to the sum of the couplings to each individual spin. In Mn_{12}-acetate the application of this

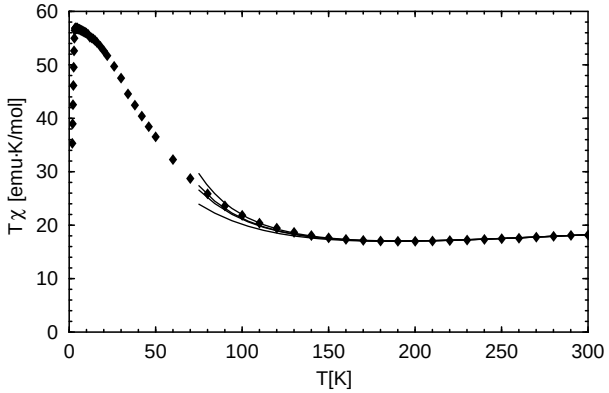

FIG. 8: Static magnetic susceptibility measured with an applied field of 0.1 T (points) and the best fit by obtained by high-temperature series expansion (solid lines). The parameter set used is given in eq. (10). The solid lines are obtained from different approximations to the 8th-order high-temperature series, and represent the error estimate for the extrapolation procedure.

analytical approach is complicated by two factors: first, the susceptibility is still far from its high-temperature limit when the sample decomposes above 300 K, and second, a number of the coupling coefficients to be determined may be of similar magnitude.

We begin by showing our measurements of the magnetic susceptibility of Mn_{12}-acetate, which are given by the symbols in Fig. 8. This measurement was performed on a 50 mg powder of the fully deuterated sample, over a temperature range of 1.8-300 K and with an applied field of 0.1 T, using a Quantum MPMS XL-5 magnetometer, and the data were corrected for diamagnetic contributions. Our data is very similar to that obtained in Ref. 54, with the exception of the dip at the lowest temperatures, which is significantly sharper in our 0.1 T measurement because the spread of sublevels in the $S = 10$ ground state is narrower than in an applied field of 1 T.[54] We comment that the presence of a small component of a faster-relaxing species of Mn_{12}-acetate molecules, estimated at 3-4% in Ref. 7, would be visible only at the lowest temperatures.

The measured susceptibility is then fitted in the form

$$T\chi(T) = \sum_{n=0}^{\infty} \tilde{C}_n \, T^{-n} \, . \qquad (9)$$

Making use of the g-values obtained for Mn_{12}-acetate by EPR measurements on a powder sample,[21] we begin by fixing the value of the leading coefficient as $\tilde{C}_0 = 30.5$ emu K mol^{-1}. The higher coefficients $\tilde{C}_n$, $n \geq 1$, are then determined from a fit to the high-temperature part of the data, from which one may obtain an estimate of the uncertainty in the coefficients from their variation with the temperature range used for the fit.

The interaction parameters J_1, J_2, J_3, and J_4 are then fitted by comparing the coefficients C_n and $\tilde{C}_n$ in Eqs. (7) and (9). Because this is an overconstrained problem, and in order to satisfy the condition that the ground state be $S = 10$, we have optimized a suitability function. This function was in turn defined as a sum of differences of appropriately rescaled coefficients C_n and $\tilde{C}_n$, $1 \leq n \leq 6$, normalized by the estimated uncertainties in the latter coefficients. The single most important piece of information which can then be extracted is $\tilde{C}_1$, which is given by a weighted sum of the interactions (see Eq. (8)) and hence sets the overall energy scale of the problem.

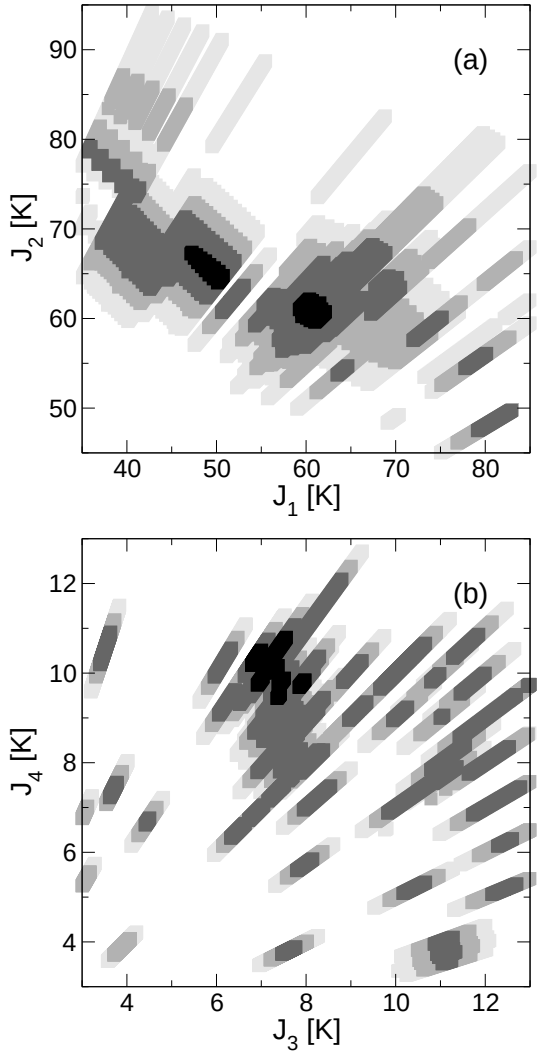

FIG. 9: Suitability of parameter sets giving a ground state of spin $S = 10$ for fitting the high-temperature susceptibility data: (a) as a function of J_1 and J_2 for all values of J_3 and J_4; (b) as a function of J_3 and J_4 for all values of J_1 and J_2. Darker shades indicate superior agreement with $\chi(T)$.

The result of this analysis for fixed $\tilde{C}_0 = 30.5$ emu K mol^{-1} is shown in Fig. 9. Each point in this figure is a projection of a point in the four-dimensional parameter space yielding an $S = 10$ ground state. Fig. 9(a) shows a projection of the four-dimensional parameter space onto the (J_1, J_2) plane and Fig. 9(b) onto the (J_3, J_4) plane.

The suitability of the parameter sets for describing the measured susceptibility $\chi(T)$ is shown by shading of the points, where darker shades denote higher and lighter shades lower levels of agreement. In Fig. 9(a) we observe two maxima of suitability. The left maximum gives rise to $S = 11$ excitations with energies of approximately 250 K ($\approx$ 21.5 meV), an energy range in which from Sec. III F no such excitations are expected, and thus we focus on the other maximum. We conclude that the requirements for an $S = 10$ ground state, for matching the susceptibility $\chi(T)$, and for $S = 11$ excitations of sufficiently high energies, constrain the exchange parameters (to within uncertainties of order 3–4 K), to the values $J_1 \approx J_2 \approx 61$ K, $J_3 \approx 7.5$ K, and $J_4 \approx 10$ K (Fig. 9).

In this region of parameter space, we have further optimized a definitive set of exchange interactions by considering the magnetic excitations, which are discussed in detail in Sec. IV D. The primary constraint set by the INS measurements presented in Sec. III is the requirement that the lowest $S = 11$ excitation have an energy of at least 285 K ($\approx$ 25 meV). This condition moves the optimal parameter set away from the minima of the suitability function found in Fig. 9 for the illustrative fitting procedure with fixed $\tilde{C}_0$, yielding the set

$$J_1 = 67.2 \text{ K } (5.79 \text{ meV}),\ J_2 = 61.8 \text{ K } (5.33 \text{ meV}),$$
$$J_3 = 7.8 \text{ K } (0.67 \text{ meV}),\ J_4 = 5.6 \text{ K } (0.48 \text{ meV}). \quad (10)$$

We will focus henceforth on this parameter set, and begin by justifying it as our final choice. For this purpose we present a direct comparison of the magnetic susceptibility obtained with the parameters of Eq. (10) and the experimental data. Instead of fixing the precise value of the zeroth-order coefficient we use this as a further fitting parameter, obtaining the slightly modified coefficient $\tilde{C}_0 = 29.5$ emu K mol^{-1}. This value corresponds to an effective average g-factor $g_{\rm eff} = 1.935$, and the modification can be interpreted as arising from single-ion anisotropies which are not otherwise present in the analysis (Sec. III F). In addition, we now use all eight orders of the high-temperature expansion, two more than were used in the calculation of the suitability function shown in Fig. 9. The lines in Fig. 8 show several Padé approximants to the series obtained from the optimal parameter set. Without entering into the technical details of this procedure, we note only that the different Padé approximants to the series allow an estimate of the uncertainty in the extrapolation of the high-temperature expansion. The divergence of the different approximants below 150 K, and the departure from the data at low temperatures, are to be expected in a high-temperature series expansion. Within the uncertainty of the extrapolation, we find good agreement with the data over the entire temperature range from approximately 80 K to 300 K. In the high-temperature regime which is relevant for our analysis, the effect of a small concentration of faster-relaxing species, i.e. of molecules with slightly different exchange constants, would be negligible both in the suitability of the fit and in comparison with the other sources of uncertainty. We stress that the overall agreement is in fact better than that provided by the maxima in Fig. 9 under the constraint $\tilde{C}_0 = 30.5$ emu K mol^{-1}. We conclude that the optimized parameters of Eq. (10) provide a good description of the experimental data for the magnetic susceptibility.

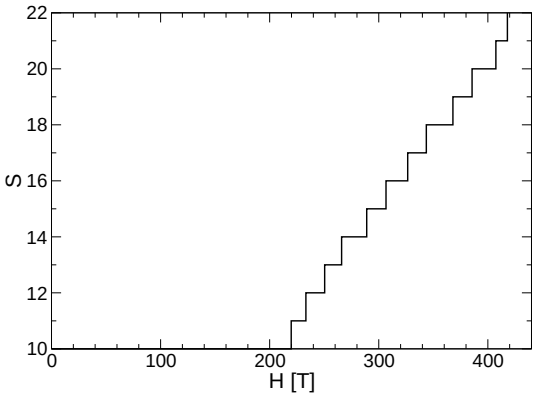

FIG. 10: Calculated magnetization curve for a Mn_{12}-acetate cluster with exchange parameters given in eq. (10).

C. High-field Magnetization

We comment here that the constraint on the overall magnitude of the interaction parameters provided by fitting the susceptibility requires a new interpretation of the high-field magnetization data.[38,39] The fixed value of the weighted sum of exchange constants C_1 has a direct correspondence to the saturation field of the system, at which all bonds must be polarized ferromagnetically. The predicted $T = 0$ magnetization curve, by which is meant here the spin $S \sim M/g\mu_{\rm B}$ as a function of applied field H, is shown in Fig. 10 for the parameters of Eq. (10), using the same value $g_{\rm eff} = 1.935$ as for the susceptibility to express the magnetic field H in units of T. The low-field data is consistent with that of Refs. 38,39, in that the $S = 10$ ground state persists up to fields in excess of 200 T. The relatively large number of narrow steps in the calculated magnetization may then also be compared with the regularly spaced steps in the data. The location of the first step, corresponding to the transition between $S = 10$ and $S = 11$ ground states, may not be underestimated from our computation by more than 10–20 T. The optimal susceptibility fit therefore implies peaks in the dM/dH data at fields smaller than the lowest peaks assigned and used to determine the exchange parameters $\{J_i\}$ in Ref. 44. However, we believe that the raw experimental data[38,39] do not in fact exclude further peaks in the region between 200 and 300 T.

The uncertainty due to errors in the exchange constants may accumulate to a value on the order of 100 T for the saturation field, which is the transition between $S = 21$ and 22 ground states, but larger devia-

tions become increasingly unlikely given the constraint on the overall energy scale obtained from the susceptibility. Hence the single largest peak in the dM/dH data of Refs. 38,39, which appears at 520 T, occurs at or above the predicted saturation. Indeed, none of the magnetization curves which we have computed yield indications for a single step which would be substantially more pronounced than all of the other steps. Given the reliability of a susceptibility measurement, and the destructive nature of the explosive compression technique involved in the high-field magnetization measurement, we suggest that the former is more representative. In this interpretation, all signals at and beyond the largest peak at 520 T in the dM/dH data would correspond to times when the sample or other components of the experimental apparatus are already disintegrating.

D. Excitation Spectrum

We turn next to an analysis of the excited states. Table III shows the lowest nondegenerate magnetic energy levels for a cluster with the optimized set of exchange interactions (10). These levels are labeled by their spin and spatial symmetry sectors. Qualitatively, the parameter values can be seen to provide a number of low-lying $S = 9$ states, as required for comparison with INS data [transitions (I) and (II)], without permitting the existence of an $S = 11$ state or additional $S = 10$ states below a significantly higher energy, whose value is in agreement with the limits set by INS [transition (III)] and high-field magnetization measurements. The fact that five nondegenerate $S = 9$ states are found in the low-energy manifold may be justified by straightforward considerations based on a spin-wave description (Sec. IV E), and can be used as an aid to experimental interpretation (Sec. III F). By considering the symmetry of the $S = 9$ states one may also observe which of these would be sensitive to a breaking of fourfold cluster symmetry, and thus by comparison with the width of the observed INS peaks establish an approximate upper bound on the extent of any such departure from symmetry (Sec. IV E).

TABLE III: Magnetic energy level spectrum obtained for the first 17 nondegenerate states with $S \geq 9$ of a Mn_{12}-acetate exchange model with the parameters of Eq. (10), classified according to spin state, level degeneracy, and spatial symmetry sector. No energetic correction is applied for uniaxial anisotropy of the cluster.

Spin S	Energy [K]	Degeneracy	Symmetry k
10	0.00	1	0
9	28.48	2	$\pm\pi/2$
9	44.47	1	π
9	91.46	1	0
9	119.67	2	$\pm\pi/2$
9	159.61	1	π
11	285.58	1	0
10	293.74	2	$\pm\pi/2$
10	297.30	1	π
11	303.23	2	$\pm\pi/2$
9	304.45	1	0
9	304.65	1	π
9	306.73	2	$\pm\pi/2$
9	307.14	1	π
10	311.11	1	0
10	317.28	1	0
9	324.51	1	0

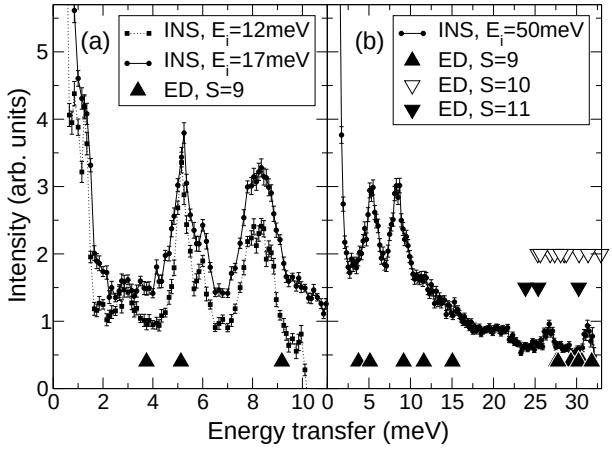

FIG. 11: Comparison with INS data of the location of calculated magnetic excitations, obtained using the optimal parameter set (10). An anisotropy correction is applied by using Eq. (3) with a single D value for all (ground and excited) states of each total spin $S = 9$, 10, or 11. The experimental data was obtained on MARI at (a) low energy transfer [Figs. 3(b) and (c)] and (b) high energy transfer [Fig. 3(a)].

A quantitative comparison between the numerical results and the positions of the excited levels observed by INS requires that the single-ion anisotropy terms be taken into account. As stated above, we have included these terms only at the level of an effective uniaxial anisotropy acting on the cluster spin [Eq. (3)]. The results of this exercise are shown in Fig. 11. With regard to position, type, and number of groups of peaks, the properties of the model are in good accord with the measured data sets. Levels (Ia), (Ib) and (IIa) deviate by no more than 20 K (≈ 2 meV) from the theoretical results while the discrepancy for levels (IIb) and (IIc) is somewhat larger. In this regard, we note that the anisotropy shift is on the order of 15 K (≈ 1.3 meV) and that rather small changes (of order 1 K) in the values of any individual coupling parameter J_i may cause large (of order 10 K), albeit not entirely uncorrelated, changes in the positions of the different excited states. Further optimization would require a full analysis of the uniaxial anisotropy at the single-ion level. Although computation of spectra for a number of selected parameter sets with the inclusion of single-ion terms is possible with current computing technology, it is a demanding numerical task due to the fact that S_z is not a conserved quantum number in this

case. As a consequence the full optimization of parameters would no longer be possible, and for this reason we do not pursue single-ion terms further here; the energy scale of the resulting mixing and splitting of levels in different manifolds remains small on the scale of the variability present in the exchange interactions. We thus focus on the robust features which may be extracted at the current level of refinement, namely a reproduction of the properties of the peak groups (I), (II), and (III) (Fig. 11).

In addition to the position of the magnetic excitations it is important also to compute their intensities to ensure that transitions to all of the calculated levels are allowed. We have computed the matrix elements $\langle g(10,9)|S_i^z|e_n(9,9)\rangle$, which by spin rotation symmetry are related directly to the elements of the operator S_i^- appropriate for the spin-flipping action on the $S = 10$ ground state $|g(10,10)\rangle$ of a neutron-scattering process, for all sites $i = 1, \ldots, 12$ of the cluster. These elements may be used in a calculation including the structure factor of the molecule to obtain the transition matrix element at any wave vector $\boldsymbol{Q}$. In Table IV we show only the incoherent sum (no phase factor) of the squares of the site matrix elements: this is sufficient to show that none of the levels is excluded for symmetry reasons, and that all may be expected to have similar weights. However, as a result of the degeneracy of the pairs $(|e_1\rangle, |e_2\rangle)$ and $(|e_5\rangle, |e_6\rangle)$, for INS purposes the relevant quantity would be the sum of these two weights. One may then expect two peaks whose integrated intensity is double that of the other three, a result certainly not inconsistent with the INS data.

We conclude this section by computing the spin distribution of the ground-state wave function. Table V shows the values of $(S_i^z)^2$ on the core $S = 3/2$ spins (i = 1, 4, 7, 10; Fig. 2), on the $S = 2$ crown spins coupled to one core spin by exchange parameter J_1 (i = 2, 5, 8, 11), and on the $S = 2$ crown spins coupled to two core spins by exchange parameter J_2 (i = 3, 6, 9, 12). The remarkable feature of these results is that approximately 90% of the spin weight of the crown spins is in the classical ferrimagnetic state invoked in Sec. II B to justify the S = 10 ground state. This value drops only to 80% for the core spins, whose mutual coupling is weak but frustrating. The degree of overlap with the classical state is confirmed by considering the S_z correlations between neighboring inequivalent sites (Table V).

The classical alignment is ensured by two factors. The first is the dominance of the exchange couplings J_1 and J_2, which forces all of the core spins be antiparallel to the crown spins, and therefore mutually FM. The weaker, frustrating J_3 and J_4 bonds then cause only minor deviations from the classical state. The second is the near-equivalence of the interactions J_1 and J_2, to which the sensitivity of the system is shown by the size of the black region in Fig. 9(a). The effect of a departure from this equivalence is illustrated by the example of the J_1-dominated parameter set originally proposed in Ref. 16, where sites i = 1, 2, 4, 5, 7, 8, 10, and 11 would be coupled to form effective $S = 1/2$ units, and only very small ordered spin components would be observed on these. Precisely because corrections of this form are small in Mn_{12}-acetate, one may expect that a spin-wave description of the excited states[55] is in fact meaningful despite the small size of the system. Finally, the relative lack of quantum mechanical fluctuation effects may also be ascribed in part to the "large" values of the ionic spins (S = 3/2 or 2, as opposed to $S = 1/2$).

E. Spin-wave Analysis

We have found that the optimal parameter set for Mn_{12}-acetate yields a ground state whose spin distribution can be said to be "80-90% classical". This result, which may seem surprising for a relatively small, quantum system, is a consequence of the fact that the two dominant exchange interactions, J_1 and J_2, are unfrustrated. The observation that an $S = 10$ ground state may be found only in a very small region of four-dimensional parameter space around this rather special limiting case is evidence that any significant frustrating interactions J_3 or J_4, or deviations from $J_1 \approx J_2$, would in fact destroy the classical ground state. The gap to the lowest excited states of the exchange model without anisotropy, measured as being approximately 4 meV (40K) in Mn_{12}-acetate [Eq. (5), Fig. 7], may also be considered as a sensitive indicator of the proximity of any similar parameter set to a ground state of a different spin $S \neq 10$.

One consequence of this quasi-classical nature is that

TABLE IV: Incoherent sum of squared matrix elements $M_n = \sum_i |\langle g(10,9)|S_i^z|e_n(9,9)\rangle|^2$ between ground and excited states for the 7 low-lying $S = 9$ levels, obtained with the parameters of Eq. (10).

n	Energy [K]	M_n
1, 2	28.48	0.25506
3	44.47	0.21426
4	91.46	0.19241
5, 6	119.67	0.19485
7	159.61	0.17911

TABLE V: Spin distribution of the ground state of Mn_{12}-acetate, characterized by the values of $(S_i^z)^2$ on all sites and by spin correlations between neighboring inequivalent sites, obtained with the parameters of Eq. (10).

$\langle g(10,10)\|(S_i^z)^2\|g(10,10)\rangle$	1.77542	i = 1, 4, 7, 10
	3.63387	i = 2, 5, 8, 11
	3.55449	i = 3, 6, 9, 12
$\langle g(10,10)\|S_i^z S_j^z\|g(10,10)\rangle$	−2.40483	$i = 1$, $j = 2$
	−2.32373	$i = 1$, $j = 3$
	3.45023	$i = 2$, $j = 3$

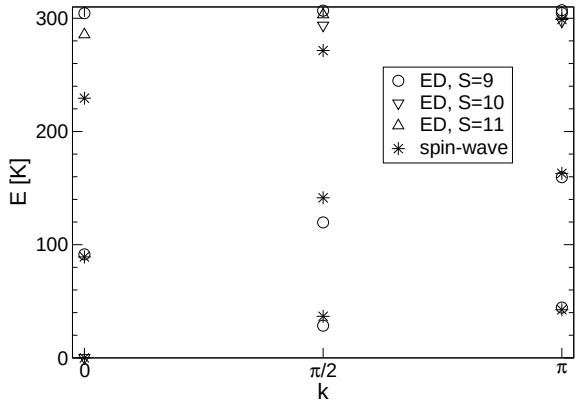

FIG. 12: Comparison between magnetic excitations calculated by exact diagonalization (ED) and within a spin-wave approximation using the parameter set of Eq. (10). No uniaxial anisotropy is included. Higher $S = 9$ and 10 excitations not included within the 3 spin-wave branches enter only at the highest energy of the $S = 11$ branch.

the magnetic excitations may be considered by conventional spin-wave theory. Within this treatment, first presented in Ref. 55, the cluster is considered as a ring of 4 unit cells each with 3 inequivalent sites. Two of the spin-wave branches correspond to reduction of the spin component $S_z = 2$ on the crown sites, leading to an $S = 9$ state of the classical cluster, while the third corresponds to an increase of the component $S_z = -3/2$ on the core sites, leading to an $S = 11$ state. The 4-cell ring has 3 inequivalent k points, where k is an effective wave vector around the ring, whence one expects 9 levels in 3 branches: the ground state, 5 $S = 9$ states, and 3 $S = 11$ states. The exact energy levels for any parameter set $\{J_i\}$ may be computed by exact diagonalization, and in Fig. 12 we show the comparison between these levels and the spin-wave approximation for the optimal Mn_{12}-acetate set (10). The agreement is remarkably good for such a crude approximation to a small quantum system, again because of the special, "classical" set of exchange interactions found in Mn_{12}-acetate. The authors of Ref. 55 applied their approximate treatment to the parameter set of Sessoli *et al.*,[16] for which the ground state deviates strongly from the classical paradigm, and unsurprisingly a correspondence between their excited states and the exact results is difficult to establish in this case. Returning to the interpretation of the INS data, the peak groups I and II (see Table II) can be identified respectively with the first and second branches of spin-wave excitations, all of which have spin $S = 9$ and provide the appropriate symmetry sectors (k in Table III).

The success of the spin-wave approximation in the physical parameter regime may be used for two further purposes. One is to investigate the sensitivity of the computed excitations to changes in individual interaction parameters without the need for a lengthy numerical calculation. We have performed this exercise in order to obtain the optimized parameter set (10), and also to observe the relative changes of different excited levels with the parameters. Here the fact that certain excitation energies change together suggests that a full, independent tuning of the levels to obtain exact agreement with the measured INS peaks may not be possible within a four-parameter exchange model, and that this would probably require the reintroduction of microscopic anisotropy terms neglected in the current analysis. In this connection we note only that single-ion anisotropy terms are expected to make the spin-wave branches less dispersive, which would improve the agreement with the INS results. The second purpose is to investigate the consequences of a breaking of fourfold cluster symmetry, if in fact one were present. In this case $J_{2a} \neq J_{2b}$ and $J_{4a} \neq J_{4b}$, and the degeneracy of the $k = \pm\pi/2$ states in Table III would be lifted. With reference to Table IV, these are the degenerate level pairs $(|e_1\rangle, |e_2\rangle)$ and $(|e_5\rangle, |e_6\rangle)$. From the fact that the INS data may already be fitted by 5 Gaussian peaks of rather similar widths [$\Gamma = 0.77$ meV (8.9 K) in (I) and (II)] not far from the resolution limit, the spin-wave description can be used to set upper bounds on $\Delta J_2 = |J_{2a} - J_{2b}|$ and $\Delta J_4 = |J_{4a} - J_{4b}|$ of approximately 0.1 meV (1 K).

V. SUMMARY

We have performed inelastic neutron scattering measurements up to high energies to identify and characterize the magnetic excitations of Mn_{12}-acetate. We find that all of the lowest energy levels, which occur in two groups at 5–6.5 meV (60–75 K) and 8–10.5 meV (95–120 K), appear to be $S = 9$ states. There are approximately five such levels, and their intensities do not vary by more than a factor of 2–3. Higher levels, including the lowest $S = 11$ states, are found at a significantly higher energy, namely the newly identified transition peak (III) at 27 meV (310 K), which is qualitatively consistent with the location of the first magnetization step. Taken together with the fact that the ground state has spin $S = 10$, the qualitative features of the measurements are already sufficient to restrict the interaction parameters of the cluster almost to a unique set. All of the available experimental information is reproduced by a parameter set with $J_1 \sim J_2 \sim 5.5$ meV (65 K), while J_3 and J_4 are smaller than 1 meV (10 K); refinement of the more robust quantitative features leads to the parameter set given in Eq. (10).

Essential supplementary fitting information is provided by the magnetic susceptibility, which we have computed by a systematic high-temperature series expansion. A correct reproduction of the high-temperature limit sets a constraint on the four interaction parameters which determines the overall energy scale of the couplings involved. In this context we note that the leading term may be expected from the cluster geometry and dominant couplings to be determined by the combination $J_1 + 2J_2$, which is indeed very close to the value $J_1 = 216$ K extracted in Ref. 16 on the assumption of one dominant

interaction. In fact this constraint is difficult to reconcile with the high-field magnetization data, whose saturation field should be given by a similar combination of terms. On the basis of our measurements and calculations, the largest feature in the dM/dH curve of Refs. 38 and 39 should correspond qualitatively to the saturation field.

In the consistent parameter set all four of the exchange interactions are AF. From qualitative considerations based on exchange and superexchange processes these results are fully plausible, despite the proximity of certain μ-oxo bridging angles to 90°. The quantitative similarity of J_1 and J_2 in spite of the very different types of exchange pathway involved, as well as the small but positive value of J_3, emphasize the difficulties inherent in performing *ab initio* calculations sufficiently accurate to reproduce the physical properties of complex magnetic systems. Even small deviations from these values are sufficient to change the spin of the ground state (Sec. IV B), to bring excluded higher-spin states into the low-energy manifold, or to return a high-temperature susceptibility well outside the limits imposed by the experimental measurement.

Throughout our analysis we have focused on the qualitative features which a candidate parameter set must reproduce. At the quantitative level there are two sources of error: the first is the uncertainty in the multiparameter problem of fitting the set $\{J_i\}$ to disparate (and occasionally conflicting) pieces of data which are themselves subject to measurement errors; the second is the terms in the Hamiltonian which we have neglected, primarily exchange asymmetries, single-ion anisotropies and higher-spin interactions. Because of the first, it is manifestly not meaningful to ascribe parameter values to the second, and yet these would be required for a perfect quantitative account of an ideal magnetic excitation spectrum. Thus we have restricted our considerations to robust results and qualitative fitting, adequate at the level of groups of INS peaks. These conditions are in fact sufficient to identify an unambiguous set of exchange constants. Although for reasons of simplicity we have focused our presention on the precise values given in Eq. (10), we have performed similar analyses for small modifications of this set. From the variability of exchange parameters between sets yielding a description of similar quality, we estimate an error bar of 2–3 K for each individual exchange parameter J_i.

In conclusion, measurements of its magnetic properties allow us to establish a definitive set of intramolecular exchange interactions for Mn_{12}-acetate. The only consistent parameter set is

$$\begin{aligned} J_1 &= 67 \pm 3\text{K} \;\; (5.8 \pm 0.3\text{meV}), \\ J_2 &= 62 \pm 3\text{K} \;\; (5.3 \pm 0.3\text{meV}), \\ J_3 &= 8 \pm 3\text{K} \;\; (0.7 \pm 0.3\text{meV}), \\ J_4 &= 6 \pm 3\text{K} \;\; (0.5 \pm 0.3\text{meV}), \end{aligned}$$

where the error bars denote the order of uncertainty for each J_i. These parameters provide both a straightforward understanding of the ground state and low-energy spectrum, and a resolution of the conflicts in the existing literature.

Acknowledgments

We are grateful to D.T. Adroja (ISIS, UK), H. Mutka (ILL, France), and S. Janssen (PSI, Switzerland) for assistance during the INS experiments. We thank N. Regnault and T. Jolicoeur for helpful provision of data concerning the spin sector of the ground state in different parameter regimes. Numerical calculations of the high-temperature series were performed on the machine `cfgauss` at the computing center of the TU Braunschweig. This work was supported by the Swiss National Science Foundation, the TMR programme Molnanomag of the European Union (No: HPRN-CT-1999-00012), and by the Deutsche Forschungsgemeinschaft through grant SU 229/6-1. A.H. would like to acknowledge the hospitality of the Institute for Theoretical Physics of the University of Hannover, where part of this work was performed.

---

* Present address: Laboratoire Léon Brillouin, CEA Saclay, 91191 Gif-sur-Yvette Cedex, France
† Corresponding author: bruce.normand@unifr.ch

[1] O. Kahn, *Molecular Magnetism*, (Wiley-VCH, Weinheim, 1993).
[2] D. Gatteschi, A. Caneschi, L. Pardi, and R. Sessoli, Science **265**, 1054 (1994).
[3] R. Sessoli and D. Gatteschi, Angew. Chem. Int. Edit., **42**, 268 (2003).
[4] B. Barbara, L. Thomas, F. Lionti, I. Chiorescu, and A. Sulpice, J. Mag. Magn. Mat. **200**, 167 (1999).
[5] see for example *Quantum Tunneling of Magnetization*, edited by L. Gunther and B. Barbara (Kluwer, Dordrecht, 1994) and references therein.
[6] M. Hennion, L. Pardi, I. Mirebeau, E. Suard, R. Sessoli, and A. Caneschi, Phys. Rev. B **56**, 8819 (1997).
[7] I. Mirebeau, M. Hennion, H. Casalta, H. Andres, H.-U. Güdel, A.V. Irodova, and A. Caneschi, Phys. Rev. Lett. **83**, 628 (1999).
[8] H. Andres, R. Basler, H.-U. Güdel, G. Aromi, G. Christou, H. Büttner, and B. Rufflé, J. Am. Chem. Soc. **122**, 12469 (2000).
[9] G. Amoretti, R. Caciuffo, J. Combet, A. Murani, and A. Caneschi, Phys. Rev. B **62**, 3022 (2000).
[10] R. Caciuffo, G. Amoretti, A. Murani, R. Sessoli, A. Caneschi, and D. Gatteschi, Phys. Rev. Lett. **81**, 4744 (1998).
[11] G. Chaboussant, R. Basler, A. Sieber, S. T. Ochsenbein, A.

Desmedt, R. E. Lechner, M.T. F. Telling, P. Kögerler, A. Müller, and H.-U. Güdel, Europhys. Lett. **59**, 291 (2002).
[12] H. Andres, R. Basler, A.J. Blake, C. Cadiou, G. Chaboussant, C.M. Grant, H.-U. Güdel, M. Murrie, S. Parsons, C. Paulsen, F. Semadini, V. Villar, W. Wernsdorfer, and R.E.P. Winpenny, Chem. Eur. J. **21**, 4867 (2002).
[13] R. Basler, G. Chaboussant, A. Sieber, H. Andres, M. Murrie, P. Kögerler, H. Bögge, D. C. Crans, E. Krickemeyer, S. Janssen, H. Mutka, A. Müller, and H.-U. Güdel, Inorg. Chem., **41**, 5675 (2002).
[14] S.T. Ochsenbein, G. Chaboussant, A. Sieber, H.-U. Güdel, S. Janssen, A. Furrer, and J.P. Attfield, Phys. Rev. B **68**, 092410 (2003).
[15] R. Basler, G. Chaboussant, C. Cañada-Vilalta, G. Christou, H. Mutka, S. Janssen, F. Altorfer, and H.-U. Güdel, Polyhedron **22**, 2471 (2003).
[16] R. Sessoli, H.-L. Tsai, A.R. Schake, S. Wang, J.B. Vincent, K. Folting, D. Gatteschi, G. Christou, and D.N. Hendrickson, J. Am. Chem. Soc. **115**, 1804 (1993).
[17] R. Sessoli, D. Gatteschi, A. Caneschi, and M.A. Novak, Nature **365**, 141 (1993).
[18] A. Caneschi, D. Gatteschi, C. Sangregorio, R. Sessoli, L. Sorace, A. Cornia, M.A. Novak, C. Paulsen, and W. Wernsdorfer, J. Mag. Mag. Mat. **200**, 182 (1999).
[19] L. Thomas, F. Lionti, R. Ballou, D. Gatteschi, R. Sessoli, and B. Barbara, Nature **383**, 145 (1996).
[20] Y. Furukawa, K. Watanabe, K. Kumagai, Z.-H. Jang, A. Lascialfari, F. Borsa, and D. Gatteschi, Phys. Rev. B **62**, 14246 (2000).
[21] A.L. Barra, D. Gatteschi, and R. Sessoli, Phys. Rev. B **56**, 8192 (1997).
[22] S. Hill, J.A.A.J. Perenboom, N.S. Dalal, T. Hathaway, T. Stalcup, and J. S. Brooks, Phys. Rev. Lett. **80**, 2453 (1998).
[23] A.M. Gomes, M.A. Novak, R. Sessoli, A. Caneschi, and D. Gatteschi, Phys. Rev. B **57**, 5021 (1998).
[24] Y. Zhong, M.P. Sarachik, J.R. Friedman, R.A. Robinson, T.M. Kelley, H. Nakotte, A.C. Christianson, F. Trouw, S.M.J. Aubin, and D.N. Hendrickson, J. Appl. Phys. **85**, 5636 (1999).
[25] L. Bokacheva, A.D. Kent, and M.A. Walters, Phys. Rev. Lett. **85**, 4803 (2000).
[26] Y. Zhong, M.P. Sarachik, J. Yoo, and D.N. Hendrickson, Phys. Rev. B **62**, 9256 (2000).
[27] B. Barbara, I. Chiorescu, R. Giraud, A.G.M. Jansen, and A. Caneschi, J. Phys. Soc. Jpn **69**, Suppl. A, 383 (2000).
[28] I. Chiorescu, R. Giraud, A.G.M. Jansen, A. Caneschi, and B. Barbara, Phys. Rev. Lett. **85**, 4807 (2000).
[29] F. Luis, F.L. Mettes, J. Tejada, D. Gatteschi, and L.J. de Jongh, Phys. Rev. Lett. **85**, 4377 (2000).
[30] A. Cornia, R. Sessoli, L. Sorace, D. Gatteschi, A.L. Barra, and C. Daiguebonne, Phys. Rev. Lett. **89**, 257201 (2002).
[31] S. Hill, S. Maccagnano, K. Park, R.M. Achey, J.M. North, and N.S. Dalal, Phys. Rev. B **65**, 224410 (2002).
[32] S. Hill, R.S. Edwards, S.I. Jones, N.S. Dalal, and J.M. North, Phys. Rev. Lett. **90**, 217204 (2003).
[33] E. del Barco, A.D. Kent, E.M. Rumberger, D.N. Hendrickson, and G. Christou, Phys. Rev. Lett. **91**, 047203 (2003).
[34] K.M. Mertes, Y. Suzuki, M.P. Sarachik, Y. Paltiel, H. Shtrikman, E. Zeldov, E. Rumberger, D.N. Hendrickson, and G. Christou, Phys. Rev. Lett. **87**, 227205 (2001).
[35] J.M. Hernandez, F. Torres, J. Tejada, and E. Molins, Phys. Rev. B **66**, 161407 (2002).
[36] R. Amigo, E. del Barco, L. Casas, E. Molins, J. Tejada, I.B. Rutel, B. Mommouton, N. Dalal, and J. Brooks, Phys. Rev. B **65**, 172403 (2002).
[37] E.M. Chudnovsky and D.A. Garanin, Phys. Rev. Lett. **87**, 187203 (2001).
[38] A.K. Zvezdin, I.A. Lubashevskii, R.Z. Levitin, V.V. Platonov, and O.M. Tatsenko, Physics-Uspekhi, **41**, 1037 (1998).
[39] D. Gatteschi and R. Sessoli, in *Magnetism: Molecules to Materials III*, edited by J.S. Miller, M. Drillon, (Wiley-VCH, Weinheim, 2002).
[40] M.I. Katsnelson, V.V. Dobrovitski, and B.N. Harmon, Phys. Rev. B **59**, 6919 (1999).
[41] M. Al-Saqer, V.V. Dobrovitski, B.N. Harmon, and M.I. Katsnelson, J. Appl. Phys. **87**, 6288 (2000).
[42] H. de Raedt, S. Miyashita, and K. Michielsen, Phys. Stat. Sol. (b) **241**, 1180 (2004).
[43] C. Raghu, I. Rudra, D. Sen, and S. Ramasesha, Phys. Rev. B **64**, 064419 (2001).
[44] N. Regnault, T. Jolicoeur, R. Sessoli, D. Gatteschi, and M. Verdaguer, Phys. Rev. B **66**, 054409 (2002).
[45] D.W. Boukhvalov, A.I. Lichtenstein, V.V. Dobrovitski, M.I. Katsnelson, B.N. Harmon, V.V. Mazurenko, and V.I. Anisimov, Phys. Rev. B **65**, 184435 (2002).
[46] K. Park, M.R. Pederson, and C.S. Hellberg, Phys. Rev. B **69**, 014416 (2004).
[47] A.A. Mukhin, V.D. Travkin, A.K. Zvezdin, S.P Lebedev, A. Caneschi, and D. Gatteschi, Europhys. Lett. **44**, 778 (1998).
[48] R.S. Edwards, S. Hill, S. Maccagnano, J.M. North, and N.S. Dalal, cond-mat/0302052 (unpublished).
[49] W. Marshall and S.W. Lovesey, *Theory of Thermal Neutron Scattering*, (Clarendon Press, Oxford, 1971).
[50] A. Furrer and H.-U. Güdel, J. Mag. Mag. Mat. **14**, 256 (1979).
[51] I. Tupitsyn and B. Barbara, in *Magnetoscience - From Molecules to Materials*, edited by J.S. Miller and M. Drillon (Wiley-VCH, Weinheim, 2000).
[52] N. Fukushima, A. Honecker, S. Wessel, and W. Brenig, Phys. Rev. B **69**, 174430 (2004).
[53] H.-J. Schmidt, J. Schnack, and M. Luban, Phys. Rev. B **64** 224415 (2001).
[54] A.R. Schake, H.-L. Tsai, R.J. Webb, K. Folting, G. Christou, and D.N. Hendrickson, Inorg. Chem. **33**, 6020 (1994).
[55] S. Yamamoto and T. Nakanishi, Phys. Rev. Lett. **89**, 157603 (2002).